

A Novel Algorithm for Detecting Singular Points from Fingerprint Images

Jie Zhou, *Senior Member, IEEE*, Fanglin Chen, and Jinwei Gu, *Student Member, IEEE*

Abstract—Fingerprint analysis is typically based on the location and pattern of detected singular points in the images. These singular points (*cores* and *deltas*) not only represent the characteristics of local ridge patterns but also determine the topological structure (i.e., fingerprint type) and largely influence the orientation field. In this paper, we propose a novel algorithm for singular points detection. After an initial detection using the conventional Poincaré Index method, a so-called DORIC feature is used to remove spurious singular points. Then, the optimal combination of singular points is selected to minimize the difference between the original orientation field and the model-based orientation field reconstructed using the singular points. A core-delta relation is used as a global constraint for the final selection of singular points. Experimental results show that our algorithm is accurate and robust, giving better results than competing approaches. The proposed detection algorithm can also be used for more general 2D oriented patterns, such as fluid flow motion, and so forth.

Index Terms—Singular points, topological structure, Poincaré Index, orientation field.

1 INTRODUCTION

A fingerprint is a 2D oriented ridge-valley pattern captured from a finger by inked press, capacitive sensor, optical sensor, etc. Within each fingerprint, there are usually two kinds of singular points: *cores* and *deltas*, where the ridge orientation patterns discontinue or change abruptly [1]. Fig. 1 lists six typical types of fingerprints with singular points marked. As an important topological feature for fingerprints, singular points can be used for fingerprint indexing (i.e., classification for fingerprint types) [2], [3], as well as for fingerprint alignment and orientation field modeling [4], [5], and so forth. These features also occur in other types of 2D oriented textures, such as fluid flow, optical flow, etc.

Many previous works have addressed singular point detection and analysis in fingerprint images. They can be roughly classified into two categories. The first approach is mainly based on using the Poincaré Index to consider the discontinuous orientation distribution around singular points [1], [2], [6], [7], [8]. This kind of algorithm usually calculates the sum of the orientation changes along a close circle around the point to judge whether it is a singular point. The second type of approach uses probability analysis, ridge analysis, shape analysis, or template matching [9], [10], [11], [12], [13], [14], [15], [16]. Compared with these latter techniques, Poincaré Index-based detection methods are generally more robust to image rotation and relatively simple to compute, so they are more widely used in real applications.

Poincaré Index-based algorithms usually result in many spurious detections (especially for low-quality fingerprint images), even after postprocessing. The spurious detected points can heavily degrade the performance of these algorithms in many applications. The spurious detections result because 1) the Poincaré Index feature alone is not enough for accurate singular point detection and 2) most postprocessing approaches utilize only local characteristic of singular points, which is not enough to discriminate true singular points from spurious detections caused by creases, scars, smudges, damped prints, etc. In the orientation field, some spurious detections actually have nearly the same local patterns as true singular points. To accurately distinguish the genuine singular points, global discriminative information should be incorporated into the detection. One interesting work proposed by Perona [17] is orientation diffusion, which implicitly use the global constraint of the oriented texture during the dynamic diffusion process.

In this paper, we will address singular point detection based on a novel so-called Differences of the ORIentation values along a Circle (DORIC) feature and global constraints. Compared with previous studies, the contributions of this paper lie in the following aspects: 1) We propose using the DORIC feature for singular point verification, which can provide more discriminative information to remove spurious detections and 2) based on an analysis of core-delta relationships, we propose to select the optimal combination of singular points by global constraints. The optimal singular points are chosen to minimize the difference between the detected orientation field and model-based orientation field reconstructed using the singular points. Experimental results show that using DORIC and global information, our algorithm is accurate and robust for a wide variety of fingerprint types. Compared with previous research, better detection results can be obtained with our approach.

The rest of this paper is organized as follows: Section 2 analyzes the topological structure of fingerprints. In

• The authors are with the Department of Automation, Tsinghua University, Beijing 100084, China. E-mail: jzhou@tsinghua.edu.cn, {chen-f106, gujinwei98}@mails.tsinghua.edu.cn.

Manuscript received 22 Jan. 2008; revised 6 June 2008; accepted 9 July 2008; published online 22 July 2008.

Recommended for acceptance by N.K. Rahtta.

For information on obtaining reprints of this article, please send e-mail to: tpami@computer.org, and reference IEEECS Log Number TPAMI-2008-01-0043.

Digital Object Identifier no. 10.1109/TPAMI.2008.188.

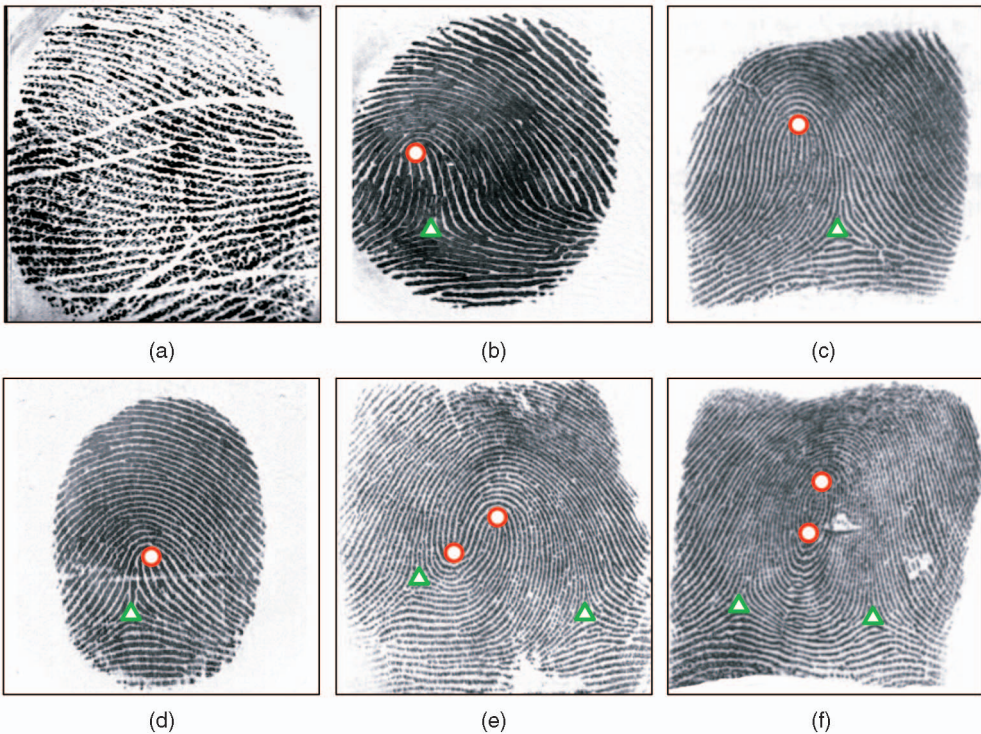


Fig. 1. Various types of fingerprints with cores (marked with circles) and deltas (marked with triangles). (a) Plain arch. (b) Tented arch. (c) Left loop. (d) Right loop. (e) Twin loop. (f) Whorl.

Section 3, the DORIC feature is proposed to remove spurious SPs. Section 4 discusses how to select the optimal combination of cores and deltas using global information. Experimental results are presented in Section 5. We finish with conclusions and a discussion of the applications of our approach in Section 6.

2 TOPOLOGICAL ANALYSIS FOR FINGERPRINT STRUCTURES

2.1 Mathematical Background

Definition. Let $V(x, y) = p(x, y) + i \cdot q(x, y)$ be a continuous 2D vector field. Then, the Poincaré Index of $V(x, y)$ along an arbitrary simple closed path γ is defined as

$$I(\gamma) = \frac{1}{2\pi} \int_{(x,y) \in \gamma} d\phi(x, y), \quad (1)$$

where $\phi(x, y) = \arg V(x, y)$ is the angle at point (x, y) and $\phi \in [0, 2\pi]$. The integration is taken counterclockwise along γ .

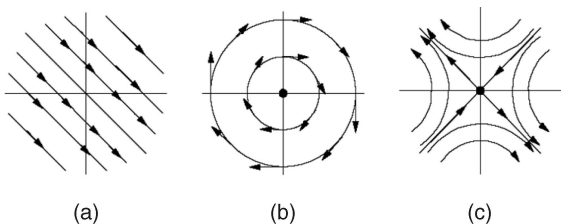


Fig. 2. Three typical patterns. (a) No singularity, $I = 0$. (b) Circle, $I = 1$. (c) Saddle, $I = -1$.

The Poincaré Index is always an integer. By computing I along a simple closed circle around a point P , one can find whether P is a singular point ($I \neq 0$) or a common point ($I = 0$). Fig. 2 illustrates the vector field and Poincaré Index for two typical low order singular points (circle point and saddle point) as well as for a region with no singular points. Refer to [18], [19], [20], [21] for more details.

Suppose that a region Ω has an exterior boundary, Γ_E , and an interior boundary, Γ_I , as shown in Fig. 3. The singular points inside Ω are denoted by the circles, $\{\gamma_i | i = 1, 2, 3, \dots\}$. C is a simple closed path inside Ω . Two important properties of the Poincaré Index can be formulated as follows and their proof can be derived from Complex Function Theory [22].

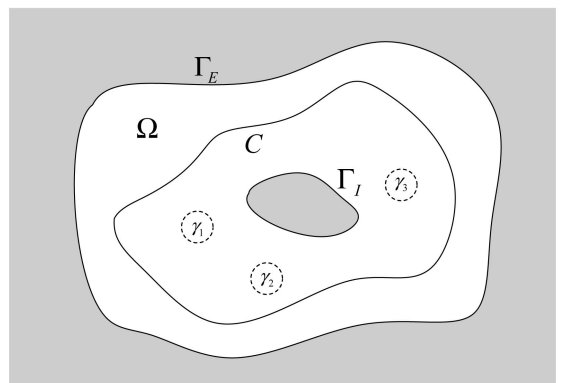


Fig. 3. Region Ω with its boundary $\partial\Omega = \Gamma_E \cup \Gamma_I$. $\{\gamma_i | i = 1, 2, 3\}$ are the circles around the singular points inside Ω . C is a simple closed path in Ω .

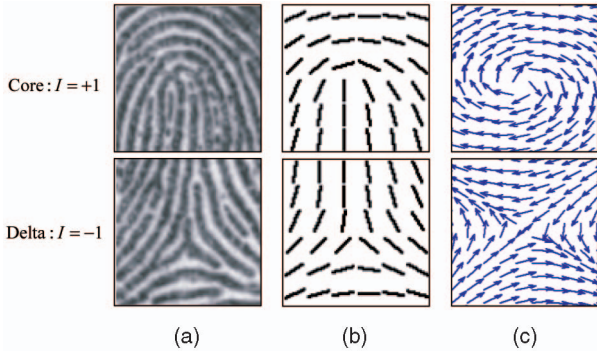


Fig. 4. (a) Singular points in fingerprints with the Poincaré Indices, (b) their local patterns in the orientation field O , and (c) the vector field V .

Property 1. The Poincaré Index along the boundary of a given region is equal to the sum of the Poincaré Indices of the singular points inside this region, i.e.,

$$\sum_k I(\gamma_k) = I(\Gamma_E) - I(\Gamma_I). \quad (2)$$

Property 2. If two simple closed paths are homotopic, and there are no other singular points between them, their Poincaré Indices are the same. For example, $I(C) = I(\Gamma_E)$, in Fig. 3.

2.2 Analysis of Fingerprint Images

For oriented texture images, such as fingerprints and fluid flow, it is natural to establish their connection with 2D topology theory. By computing the orientation field, $O(m, n)(\in [0, \pi])$, which represents the ridge orientation for each pixel, (m, n) , we can build a vector field $V = \cos 2O + i \cdot \sin 2O$ [5], [23]. Then, we can apply the above definitions and properties on these images. The singular points in fingerprints are found to be consistent with the singular points defined in topology. In Fig. 4, we list two typical singular points for fingerprints, their Poincaré Indices, and their local patterns in the orientation field O and the vector field V .

An interesting conclusion for fingerprints can be deduced based on **Property 1**. Since fingerprints usually do not have interior boundary Γ_i and only have isolated singular points (cores and deltas) with known Poincaré index (+1 for core, -1 for delta), (2) can be written as

$$N_c - N_d = I(\Gamma_E), \quad (3)$$

where N_c is the number of the cores, N_d is the number of the deltas, and Γ_E is the exterior boundary of the fingerprint.

Previous works have pointed out that cores and deltas should appear in pairs [2], [4], [5]. Two views of a real thumb are shown as an example in Figs. 5a and 5b with the cores and the deltas marked. As shown in Fig. 5, if fingerprints are captured completely, it can be assumed that the orientation of left, right, bottom, and top boundaries are nearly horizontal. For the simple closed path Γ_E consisting of this kind of boundaries, $I(\Gamma_E) = 0$, and then $N_c = N_d$.

As for **Property 2**, we know that the Poincaré Index can be computed along any simple closed path as long as it is homotopic with the closed circle around the same points. This allows us to adaptively choose the integral path for the

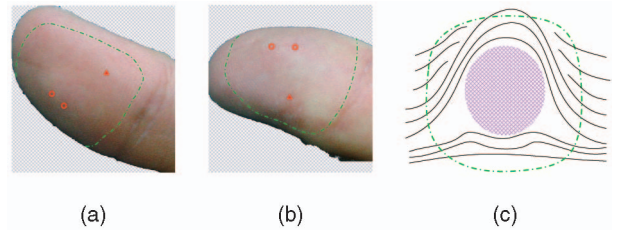


Fig. 5. (a) Left and (b) right views of a real thumb with singular points and boundary marked. (c) The boundary of a complete fingerprint abstraction.

boundary, for example, to choose the path where the orientation confidence is much higher.

3 USING DORIC FEATURE TO REMOVE SPURIOUS SINGULAR POINTS

3.1 DORIC Feature

Many previous researchers have shown that Poincaré Index-based methods can usually detect nearly all true singular points when the Index is computed along small region boundaries, but this also leads to many spurious detections. If a larger region is chosen, true singular points will be easy to miss [8]. In order to remove spurious detections while preserving a good detection rate, we propose a novel feature extended from the Poincaré Index, which can provide more discriminating features and be used to verify the trueness of each detection after using Poincaré Index algorithm.

The Poincaré Index is defined as the sum of the orientation differences along a closed circle L (in our study, its radius is chosen as 5 pixels). For a given point P , assume that the set of sampled points along L is $\{T_1, T_2, T_3, \dots, T_{N-1}\}$ and o_i is the orientation of point T_i . Then, the Poincaré Index of P can be computed by [2], [4]

$$\begin{aligned} I_P &= \frac{1}{\pi} \sum_{i=1}^{N-1} f(o_{i+1} - o_i) \\ &= \frac{1}{\pi} \sum_{i=1}^{N-1} f(\delta o_i), \end{aligned} \quad (4)$$

where $o_N = o_1$, and function f is defined as

$$f(x) = \begin{cases} x, & |x| \leq \frac{\pi}{2}, \\ \pi - x, & x > \frac{\pi}{2}, \\ \pi + x, & x < -\frac{\pi}{2}. \end{cases} \quad (5)$$

The Poincaré Index is only the sum of δo_i . It contains no information about the structure of δo_i , $i = 1, 2, 3, \dots, N-1$, and it cannot describe the singular point completely. So, when there are creases, scars, smudges, or damped prints in the fingerprint images, the Poincaré Index method will easily result in many spurious singular points. Postprocessing steps are therefore usually necessary. In our study, we use two simple heuristic rules during postprocessing: 1) If a delta is too close to a core (the distance between them is smaller than 8 pixels), remove both of them and 2) in a very small region (a circular region with a radius of 8 pixels), if there is more than one core (or delta), an average core (or delta) can be computed instead. Suppose that there are

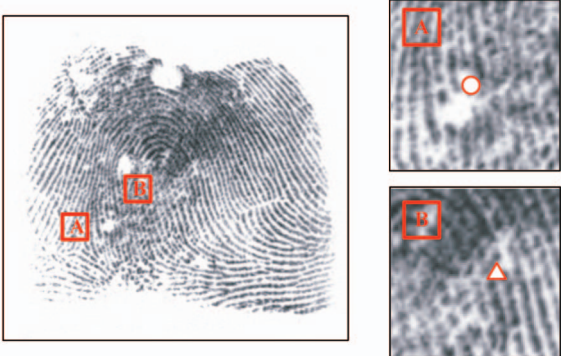


Fig. 6. Two examples of spurious singular points detected using a conventional Poincaré Index-based method and postprocessing steps, in which the false core is marked with a circle and the false delta is marked with a triangle.

N cores (or deltas) in such a region, $\{(x_i, y_i), i = 1, 2, \dots, N\}$. Then, the average core (or delta) (x, y) is computed by

$$x = \frac{1}{N} \sum_{i=1}^N x_i \quad (6)$$

and

$$y = \frac{1}{N} \sum_{i=1}^N y_i. \quad (7)$$

However, even after this postprocessing step, many spurious detections still remain. Fig. 6 shows two examples from a poor-quality fingerprint, illustrating points that are falsely detected as a core and a delta by using the Poincaré Index method and this postprocessing.

In order to further remove the spurious points, we propose to use a novel feature, which contains more information about the singular point. The feature on point P is a vector, which consists of the DORIC around P , i.e.,

$$DORIC(P) = [\delta o_1, \delta o_2, \dots, \delta o_{N-1}]. \quad (8)$$

As DORIC contains all δo_i , it can describe the singular point more completely. The Poincaré Index can be seen as the sum of DORIC features and DORIC features can be regarded as an extended form of Poincaré Index. Fig. 7 shows six singular points detected by the Poincaré Index method and their DORIC features are plotted as curves (among them, Figs. 7a, 7b, 7c, and 7d are true and Figs. 7e and 7f are spurious detections).

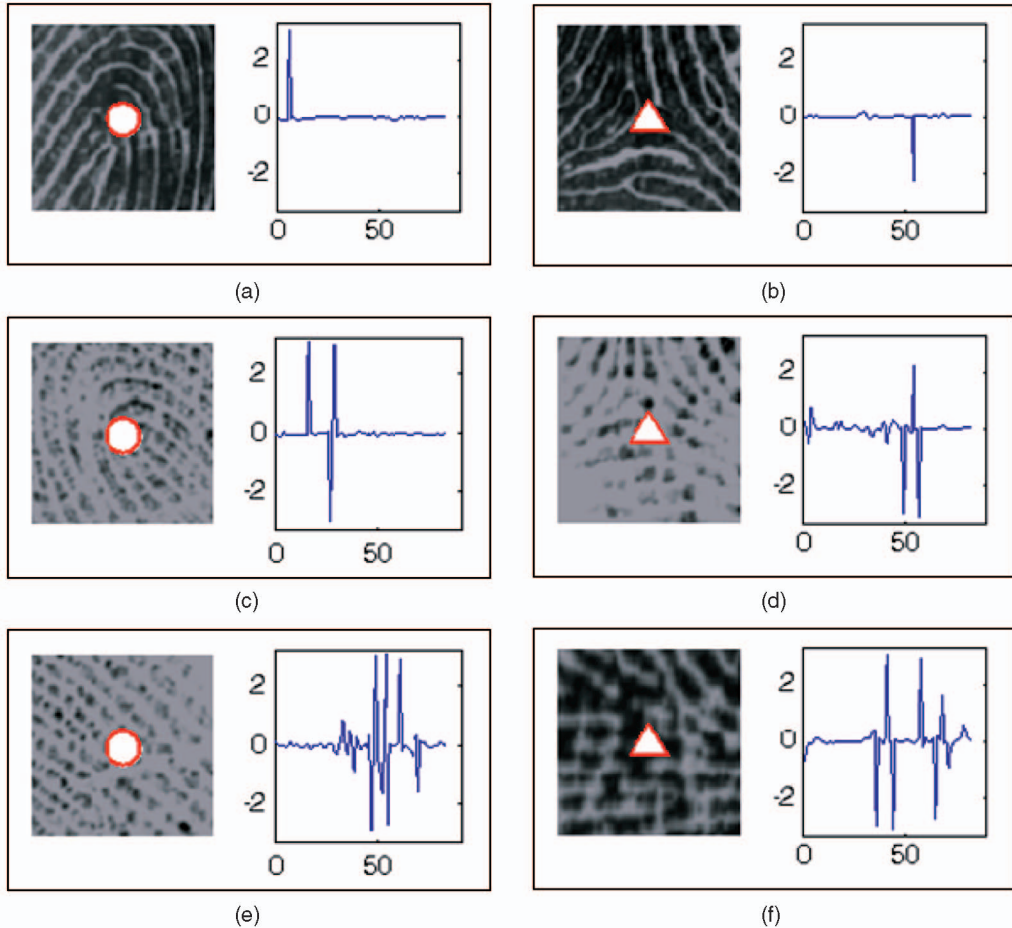


Fig. 7. Singular points detected by using the Poincaré Index algorithm and their DORIC features (plotted as curves): (a), (b), (c), and (d) are true while (e) and (f) are spurious.

Since the orientation field is defined in $[0, \pi]$, there will be one DORIC feature pulse for each singular point (positive pulse for core, and negative pulse for delta) if the orientation field is detected perfectly. See Figs. 7a and 7b for examples. Although the noise around the true singular points may change the curves a little, there exists a clearly evident difference between true and spurious singular points. These phenomena can be observed in Fig. 7.

After postprocessing steps, the detected singular points are isolated, i.e., there is only one singular point for any fairly large region. Thus, it is more appropriate to compute the DORIC features along a large circle. Then, N can be a large number, and consequently, the curves of DORIC features will be more continuous, which makes the following analysis much easier. In our study, the radius of the circle is chosen as 10 pixels.

3.2 Removing Spurious Singular Points

To distinguish true singular points from spurious ones, a two-step classifier is proposed as below.

For each point with nonzero Poincaré Index in the candidate set S , we compute its DORIC feature. If there is exactly one pulse (i.e., positive pulse for core and negative pulse for delta) with the height nearly up to π , it is a valid singular point and will be kept in the final set S of singular points; otherwise, it will be removed from candidate set S and placed into an auxiliary set S' of candidates for further processing. This process is outlined in Algorithm 1.

Algorithm 1 Pseudocode of the first step for removing spurious SPs

```

1 for each detection point  $P$  in  $S$  do
2    $DORIC(P) = [\delta o_1, \delta o_2, \dots, \delta o_{N-1}]$ ;
3   if  $\exists!k \in [1, N-1]$ , that  $|\delta o_k| > T$ , then
4     keep  $P$  in  $S$ ;
5   end
6   else
7     remove  $P$  to  $S'$ 
8   end
9 end
```

The auxiliary point set S' can contain a mixture of true singular point and spurious detections. We will design a classifier based on training samples to distinguish between the true points (e.g., Figs. 7c and 7d) and the spurious ones (e.g., Figs. 7e and 7f).

Since it is time consuming to manually label true and spurious singular point samples for the training of the classifier, we will utilize sample learning methods suitable for small-numbered samples. We have chosen to use a Support Vector Machine (**SVM**) to design our classifier. **SVMs** try to find an optimal separating hyperplane in the feature space and minimize the classification error for the training data using a nonlinear transform function [24]. **SVM** has been well studied in statistical learning theory [24], [25], [26]. Suppose that the original data space is L and the feature space is H (here, we use L as a hint for “low dimensional,” and H for “high dimensional”). Let Φ be the transforming function between the two spaces:

$$\Phi : L \mapsto H. \quad (9)$$

Let N be the number of training samples. Denoting the set of training data as $\{\mathbf{x}_i, y_i\}$, $i = 1, 2, \dots, N$, $\mathbf{x}_i \in L$, and $y_i \in \{-1, +1\}$, the **SVM** calculates the sign of $f(\mathbf{x})$ as the decision result, where $f(\mathbf{x})$ is calculated as

$$f(\mathbf{x}) = \sum_{i=1}^N \alpha_i y_i K(\mathbf{x}_i, \mathbf{x}) + b. \quad (10)$$

The nature of the decision surface is mainly defined by the kernel function $K(\mathbf{x}_i, \mathbf{x})$, which should satisfy Mercer’s conditions. The commonly used kernels include polynomial kernels $K(\mathbf{x}_i, \mathbf{x}) = (\mathbf{x}_i^T \mathbf{x} + 1)^d$, where d is a positive integer to define the degree of a polynomial decision surface, and Gaussian kernels $K(\mathbf{x}_i, \mathbf{x}) = e^{-g\|\mathbf{x}_i - \mathbf{x}\|^2}$. The kernel function $K(\mathbf{x}_i, \mathbf{x})$ can be easily computed by an inner product of the nonlinear transform function [24].

In this problem, the missed detection rate (classifying true singular points as spurious ones) should be very small. The separating hyperplane is defined by α_i ($i = 1, 2, \dots, N$) and b . In our study, we select an optimal b_0 to move the separating plane to an appropriate position that will misclassify less than 2 percent of true singular points as spurious ones and, meanwhile, minimize the error of classifying spurious singular points as true ones.

From the definition of DORIC features, we can see that this vector is sensitive to image rotation. To overcome the affect of image rotation, we augment our training set by rotating each fingerprint sample image by 10 degree increments. All of the samples are used for training the **SVM** classifier to make it insensitive to image rotation.

Based on the **SVM** result, we can make the decision whether a point P in S' should be moved back to the final candidate set S or not. After this two-step classification process, a lot of the spurious singular points are removed. For example, Figs. 7e and 7f can be successfully judged as spurious singular points while the other four are kept as true ones.

4 SINGULAR POINTS SELECTION WITH GLOBAL INFORMATION

As we pointed out earlier, local features alone are not enough to fully discriminate the true singular points from spurious detections, which can actually have similar local characteristics as the true ones. This motivates us to incorporate more global discriminative information for detection.

4.1 Removing Invalid Combinations

The core-delta relation deduced in Section 2 is used as a global constraint for selecting the optimal set of final singular points. In real applications, many fingerprint images captured by optical or capacitive sensors are not complete. Often they will lose one or two deltas. In this case, the number of cores is not necessarily equal to the number of deltas. Nevertheless, (3) still presents us a global topological constraint for singular points. Suppose the effective region of the fingerprints is Ω . By computing $I(\partial\Omega)$, we can know that only a few combinations of the singular points are valid. In Table 1, we list most of the possible combinations of singular points for fingerprints with the Poincaré Index and the possible types (PA—plain

TABLE 1
Frequent Combinations of Singular Points
in a Complete Fingerprint

$I(\partial\Omega)$	Core	Delta	Possible Types
0	0	0	PA
	1	1	LL, RL, TA
	2	2	TL, Whorl
1	1	0	LL, RL, TA
	2	1	TL, Whorl
2	2	0	TL, Whorl

arch, TA—tent arch, LL—left loop, RL—right loop, TL—twin loop).

In practice, the orientation field, O , directly extracted from the images, will contain a lot of noise due to creases, scars, blurring, etc. As shown in Fig. 8a, the original orientation field, O , is computed using the state-of-the-art hierarchical gradient-based method [27]. Although this works well in most of the effective region, there is still some noise in the marked areas, which will influence the computation of $I(\partial\Omega)$. To smooth out this kind of noise, we adopt the polynomial model-based method proposed by us in [28]. We use two bivariate polynomials, $P(x, y) = \sum_{i,j} p_{ij}x^i y^j$ and $Q(x, y) = \sum_{i,j} q_{ij}x^i y^j$, to approximate $\cos 2O$ and $\sin 2O$, respectively. The parameters, $\{p_{ij}, q_{ij}\}$, can be estimated with the Least Squares method linearly. After this approximation, the smoothed orientation field can be reconstructed as

$$O_P(x, y) = \frac{1}{2} \arctan \frac{\sum_{i,j} q_{ij}x^i y^j}{\sum_{i,j} p_{ij}x^i y^j}. \quad (11)$$

Fig. 8b shows the orientation field after smoothing. Although the polynomial-based reconstruction is not good enough at the regions near the singular points in the center of Ω , it can well model the orientation field near the boundary and effectively remove the noise and thus keep the global topological property invariant. This is just what we need to robustly compute $I(\partial\Omega)$. In Fig. 8c, the boundary of the fingerprint along with the singular points

is depicted. The results also verify our conclusion about the topological constraint about the singular points.

By computing the global Poincaré Index $I(\partial\Omega)$, we can easily remove some invalid combinations of singular points. For example, when the global Poincaré Index is equal to 1, the combinations of 1-core-0-delta and 2-core-1-delta are calculated and other situations are not considered. This speeds up the algorithm greatly.

4.2 Selection of Optimal Singular Points

As known, singular points can be used to determine the global structure of the orientation field of fingerprints. In fact, there are several orientation field models related to singular points [4], [5], [29]. Our basic idea is to select the optimal singular points by minimizing the difference between the original orientation field and the model-based orientation field reconstructed using the singular points.

Denote the original orientation field as O_0 and the reconstructed orientation field as $O(\Theta, s)$, where Θ is the model's parameter. The original orientation field, O_0 , is computed by the hierarchical gradient-based method [27]. As for the model-based reconstructed orientation field, $O(\Theta, s)$, we choose the Zero-Pole model proposed by Sherlock and Monro [4], considering both the model accuracy and the computational efficiency. This model is based on the singular points, s , which takes the cores as zeros and the deltas as poles in the complex plane. It can be formulated as

$$O(x, y; \phi, s) = \frac{1}{2} \arg \left(e^{i\phi} \cdot \frac{\prod_i (z - z_{c_i})}{\prod_j (z - z_{d_j})} \right), \quad (12)$$

where $z = x + iy$, z_{c_i} is the i th core, z_{d_j} is the j th delta, and $\phi \in [0, 2\pi]$ is a *background angle* to be decided. However, how to estimate ϕ is not mentioned in previous works. In our study, we propose estimating the background angle ϕ using a Least Square Meaning (LSM) measurement. The optimal ϕ is estimated by

$$\phi^* = \arg \min_{\phi} J(\phi), \quad (13)$$

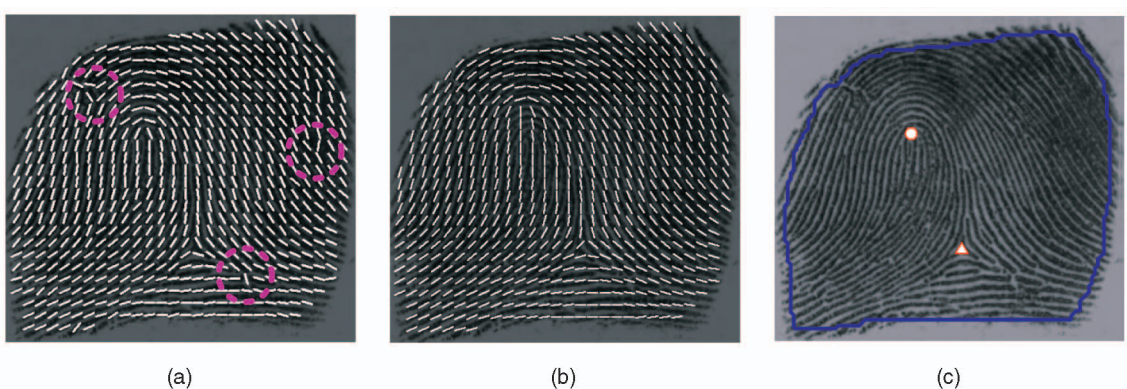


Fig. 8. Computation of the orientation field (a) by hierarchical gradient-based method [27], (b) after using polynomial model-based method [28], (c) blue curve is the boundary of the effective region, cores and deltas are marked with circles and triangles, respectively, and $I(\partial\Omega) = 0$, which means the numbers of cores and deltas may be (0, 0), (1, 1), or (2, 2).

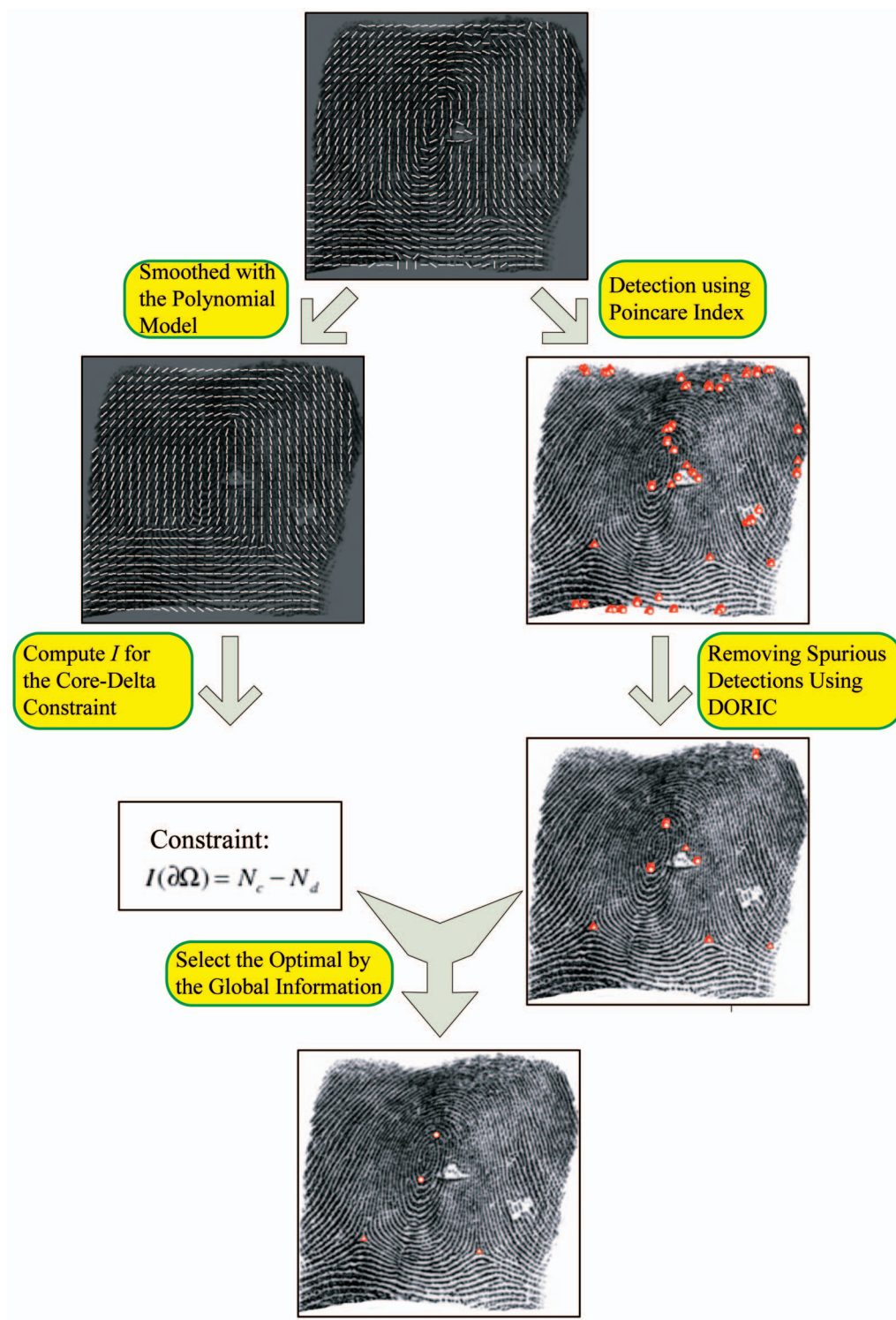


Fig. 9. Flowchart of our proposed detection method.

where

$$J(\phi) = \sum_{\Omega} (\sin(2O + \phi) - \sin 2O_0)^2 + (\cos(2O + \phi) - \cos 2O_0)^2. \quad (14)$$

Each singular point is denoted by a triple, (x, y, t) , with its positions and type (core/delta). All singular point candidates are in the set $S = \{(x_i, y_i, t_i)\}_{i=1}^M$. The set of true

singular points, s , is a subset of S . The optimal singular

points can be selected as

$$s^* = \arg \min_{s \subseteq S} \|O(\Theta, s) - O_0\|, \quad (15)$$

where the difference function, $\|\cdot\|$, is defined as $J(\phi^*)$ (see (13) and (14)). The process of singular point selection is summarized in Algorithm 2.

TABLE 2
The Performance of DORIC on NIST-4

Step	rate	Cores	Deltas	Core+Deltas
Step1: Poincaré Index	Miss rate	3.50	2.10	2.81
	False alarm rate	2078.25	2129.54	2103.55
Step2: Removing spurious SPs by DORIC	Miss rate	3.94	2.55	3.25
	False alarm rate	994.60	1027.59	1010.87

TABLE 3
The Performance of DORIC on FVC02's DB1

Step	rate	Cores	Deltas	Core+Deltas
Step1: Poincaré Index	Miss rate	0.43	0.60	0.48
	False alarm rate	228.14	683.69	348.29
Step2: Removing spurious SPs by DORIC	Miss rate	2.16	1.21	1.91
	False alarm rate	99.13	311.48	155.14

TABLE 4
The Performance of DORIC on FVC02's DB2

Step	rate	Cores	Deltas	Core+Deltas
Step1: Poincaré Index	Miss rate	0.56	0.57	0.56
	False alarm rate	938.63	2417.38	1357.55
Step2: Removing spurious SPs by DORIC	Miss rate	2.48	1.71	2.26
	False alarm rate	463.40	1275.50	693.46

TABLE 5
The Comparison Results of Different Detection Algorithms on NIST-4

		Proposed	Rule-based [1]	Tico's [7]	Ramo's [10]
Singular points (cores + deltas)	Detection rate	87.80	76.63	46.23	53.62
	False alarm rate	7.32	36.98	92.83	57.25
Cores	Detection rate	86.13	75.91	43.07	68.76
	False alarm rate	8.47	48.32	65.69	47.30
Deltas	Detection rate	89.51	77.36	49.48	38.08
	False alarm rate	6.15	25.34	120.69	67.47
Fingerprints	Correct rate	73.48	51.20	17.60	31.47

Algorithm 2 Pseudocode of the optimal selection step

```

Input: the candidate singular points set,  $S$ 
Output: the selected singular points' combination,  $s^*$ 
1 Reconstruct the orientation field  $O_p$  use polynomial model (see (11)).
2 Compute the global Poincaré Index  $I(\delta\Omega)$ .
3 Determine the candidate combinations,  $C$ , based on Table 1.

4  $e = \text{MAX}$  (a large enough number)
5 for each combination  $c$  in  $C$  do
6   Reconstruct the orientation field  $O$  using  $c$  by Zero-Pole model (see (12), (13), and (14))
7   Computer the error between  $O$  and the original orientation filed  $O_0$ :  $e_{tmp} = \|O_0 - O\|$ , where  $\|\cdot\|$  is defined as  $J(\phi^*)$  (see (13) and (14)).
8   if  $e_{tmp} < e$ , then
9      $e = e_{tmp}$ ;

```

10 $s^* = c$.

11 **end**

12 **end**

The flowchart of the whole detection algorithm is shown in Fig. 9.

5 EXPERIMENTAL RESULTS

We test the proposed method on NIST Special Database 4 (NIST-4) [30] and public fingerprint databases FVC02 DB1 and DB2 [31].

The NIST-4 contains 2,000 pairs of fingerprint images (two instances, f and s , for each entity), and the images are 512×512 with 8 bits per pixel.

Both DB1 and DB2 from FVC02 contain 800 fingerprints, i.e., 100 fingers and eight prints for each finger, respectively.

The FVC02 database has the following features:

TABLE 6
The Comparison Results of Different Detection Algorithms on FVC02's DB1

		Proposed	Rule-based [1]	Tico's [7]	Ramo's [10]
Singular points (cores + deltas)	Detection rate	96.10	77.09	76.53	86.75
	False alarm rate	4.30	29.72	30.67	15.28
Cores	Detection rate	95.78	86.26	90.27	92.19
	False alarm rate	2.27	15.92	10.78	8.47
Deltas	Detection rate	96.98	55.24	55.49	68.42
	False alarm rate	9.97	81.04	80.20	46.15
Fingerprints	Correct rate	88.88	50.00	58.50	53.54

TABLE 7
The Comparison Results of Different Detection Algorithms on FVC02's DB2

		Proposed	Rule-based [1]	Tico's [7]	Ramo's [10]
Singular points (cores + deltas)	Detection rate	94.51	58.78	50.81	71.03
	False alarm rate	9.60	70.13	96.83	40.79
Cores	Detection rate	95.95	73.86	65.38	80.72
	False alarm rate	8.45	35.40	52.94	23.88
Deltas	Detection rate	90.88	37.61	34.75	37.50
	False alarm rate	12.54	165.85	187.80	166.67
Fingerprints	Correct rate	81.25	56.57	32.32	49.49

1. fingerprints collected in three sessions with at least two weeks time separating each session;
2. no efforts were made to control image quality and the sensors were not systematically cleaned;
3. at each session, four impressions were acquired for each of the four fingers of each volunteer;
4. during the second session, individuals were requested to exaggerate displacement (impressions 1

and 2) and rotation (3 and 4) of the finger, not to exceed 35 degrees;

5. during the third session, fingers were alternatively dried (impressions 1 and 2) and moistened (3 and 4).

We chose 360 fingerprints for training data (320 fingerprints from FVC00 DB1_b, DB2_b, DB3_b, DB4_b, and 40 fingerprints from the NIST Special Database 14), which is only used for the SVM-based DORIC feature classifier. The fingerprints in the training set are different from the testing set. After the Poincaré Index-based method, singular points are manually labeled as true or spurious and then used for training the SVM.

The singular points of all of the fingerprints in the testing database are manually labeled beforehand to obtain ground truth. For a ground truth singular point, $(x_0; y_0; t_0)$, if a detected singular point, $(x; y; t)$, satisfies $t = t_0$, $|x - x_0| < 5$ (pixels), and $|y - y_0| < 5$ (pixels), it is said to be truly detected and, otherwise, it is called a miss. The detection rate is defined as the ratio of truly detected singular points to all ground truth singular points. The miss rate is defined as the ratio of the number of missed singular points to the number of all

TABLE 8
The Comparison Results with Chikkerur and Ratha [16] on NIST4

		Proposed	Chikkerur's
Singular points (cores + deltas)	Detection rate	87.80	86.02
	False alarm rate	7.32	9.32
Cores	Detection rate	86.13	85.40
	False alarm rate	8.47	9.93
Deltas	Detection rate	89.51	86.66
	False alarm rate	6.15	8.70
Fingerprints	Correct rate	73.48	71.33

TABLE 9
The Comparison Results with Chikkerur and Ratha [16] on FVC02's DB1

		Proposed	Chikkerur's
Singular points (cores + deltas)	Detection rate	96.10	95.06
	False alarm rate	4.30	7.25
Cores	Detection rate	95.78	95.89
	False alarm rate	2.27	6.93
Deltas	Detection rate	96.98	92.75
	False alarm rate	9.97	8.16
Fingerprints	Correct rate	88.88	85.13

TABLE 10
The Comparison Results with Chikkerur and Ratha [16] on FVC02's DB2

		Proposed	Chikkerur's
Singular points (cores + deltas)	Detection rate	94.51	93.46
	False alarm rate	9.60	17.33
Cores	Detection rate	95.95	93.23
	False alarm rate	8.45	13.87
Deltas	Detection rate	90.88	94.20
	False alarm rate	12.54	28.62
Fingerprints	Correct rate	81.25	73.25

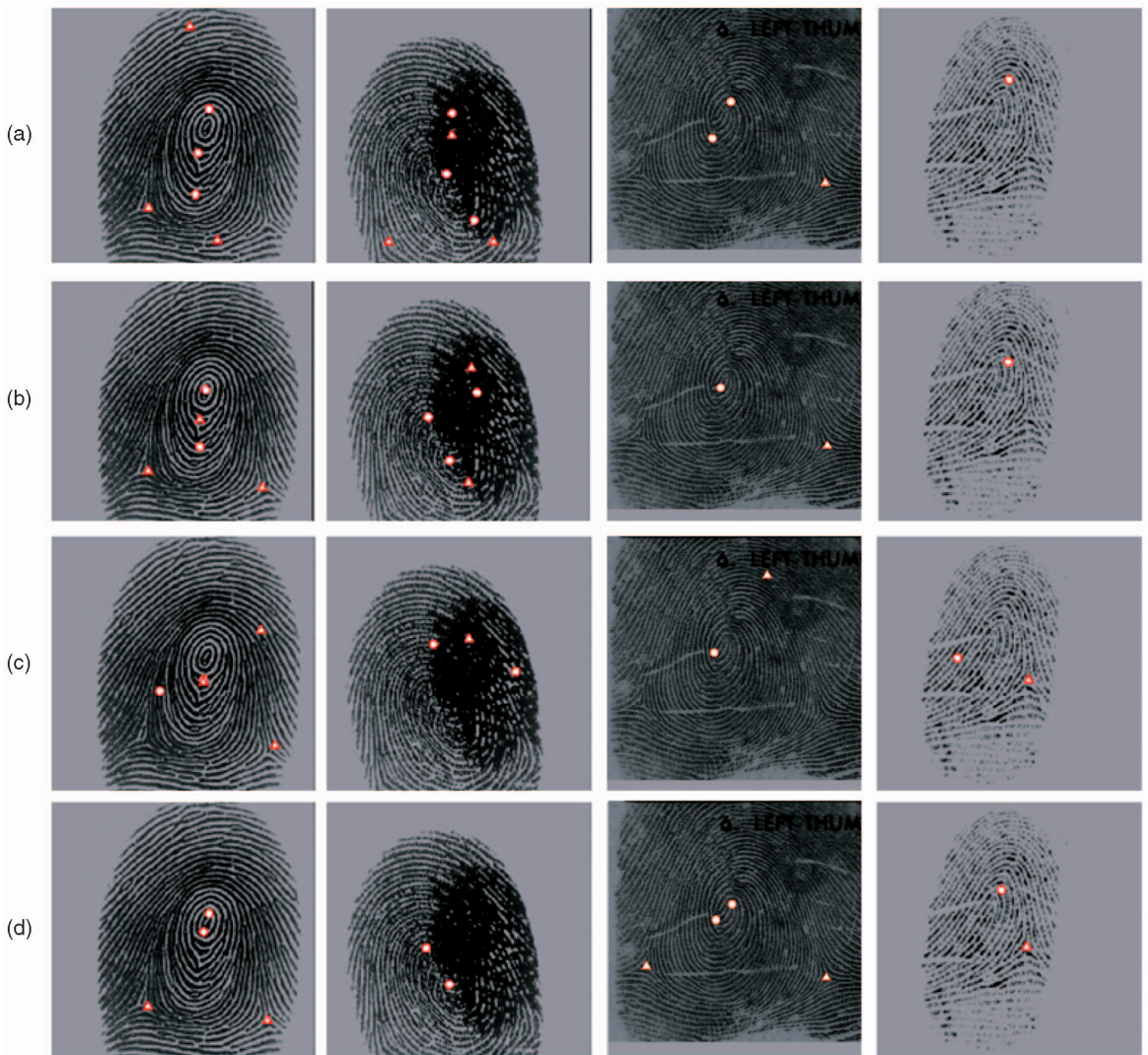


Fig. 10. Some comparison results of singular point detection. The four rows (from top to bottom) show the detected results using the rule-based algorithm [1], Tico's algorithm [7], Ramo's algorithm [10], and the proposed algorithm, respectively.

ground truth singular points. It can be seen that the sum of detection rate and miss rate is 1 or 100 percent. The false alarm rate is defined as the number of falsely detected singular points versus the number of all ground truth singular points. If all singular points are detected and there are no spurious singular points in a fingerprint, the fingerprint is said to be "correctly" detected (see the last row in Tables 5, 6, 7, 8, 9, and 10).

We perform singular point detection according to the algorithm shown in Fig. 9. The effective region is extracted by computing the mean and the variance of the intensity value on each block and doing simple binarization (an "effective" block should have the mean in [20, 220] and the variance greater than 6 in our study). Morphological operators including dilation and erosion are made to remove some isolated points and to fill large holes. The order of the polynomials is set to 4 in the orientation-field-smoothing step.

5.1 Performance of the Doric Feature

The performance of removing spurious singular points using DORIC is listed in Tables 2, 3, and 4. The first two

steps of the proposed algorithm are: the Poincaré Index method (Step 1) and removing spurious singular points by DORIC (Step 2). For each table, the "miss rate" and "false alarm rate" of Step 1 and Step 2 are shown. From the result, it can be seen that a large percentage of the spurious SPs can be removed by using DORIC features.

5.2 Comparison with Other Poincaré Index-Based Methods

We have also compared the proposed detection algorithm with some conventional Poincaré Index-based algorithms. Since our algorithm is developed from the Poincaré Index, we first chose three widely used Poincaré Index-based algorithms for comparison, including a rule-based algorithm [1], Tico's algorithm [7], and Ramo's algorithm [10]. The comparison results are listed in Tables 5, 6, and 7. In Fig. 10, we present the detection results on some typical fingerprints, which suffer the difficulties of creases, scars, smudges, dryness, damped or blurred prints, etc. The four rows (from top to bottom) show the detected results using rule-based algorithm [1], Tico's algorithm [7], Ramo's algorithm [10], and the proposed algorithm, respectively.



Fig. 11. Detecting vortexes and saddles in the fluid image using the proposed algorithm.

From these results, we can see that the singular points can be more robustly detected by using the proposed algorithm and the detected positions are reasonably accurate.

5.3 Comparison with Non-Poincaré Index-Based Method

There are also many other methods of singular point detection, among which, the recent technique based on complex filtering has been reported to obtain a better performance than others. Nilsson et al. [14], [15] first proposed the approach based on complex filtering, which relies on detecting the parabolic and triangular symmetry associated with core and delta points. Chikkerur and Ratha [16] improved the technique by using three additional certainty maps that represent heuristics about the likely positions and orientations of cores and deltas.

To give a completely comparative study, we also compare the proposed algorithm with that of Chikkerur and Ratha [16]. The comparison results are listed in Tables 8, 9, and 10. These results show that the proposed algorithm has a better performance. The proposed algorithm has a higher detection rate and lower false alarm rate for singular points (cores + deltas), and a much higher correct rate for whole fingerprints. Based on these results, our algorithm shows a satisfactory performance for real applications.

The proposed method is suitable for real-time processing. Both the polynomial-based smoothing and the selection with the global orientation field can be done linearly by Least Squares Method. The Zero-Pole model-based reconstruction does not take much time and the topological constraint and DORIC feature effectively remove lots of spurious detections. Our algorithm is currently implemented with Matlab and C on an AMD 2200 Hz 512 Mbyte PC without optimization. The average processing time for each fingerprint is around 0.10 second. This makes the proposed algorithm feasible for real applications.

It should be mentioned that the proposed algorithm can also be utilized for the detection of singular points in other fields. For example, we can use it to detect vortexes and saddles in a fluid image (see Fig. 11 for an example).

6 CONCLUSION

To sum up, we have focused on the detection of singular points in fingerprints in this paper. Our contributions lie in two aspects. 1) We propose a new feature, DORIC, in addition to the Poincaré Index, which can effectively remove spurious detections and 2) we take the topological relations of singular points as a global constraint for fingerprints and propose a novel algorithm for singular point detection using the global orientation field. The optimal singular points can be selected by minimizing the difference between the original orientation field and the model-based orientation field reconstructed from the singular points. Experimental results have shown that the proposed algorithm is effective for singular point detection, better than the reported best results.

ACKNOWLEDGMENTS

An early version of this manuscript was published in the *Proceedings of the International Conference of Biometrics* (pp. 261-270, 2007). This work was supported by the National 863 Hi-Tech Development Program of China under Grant 2008AA01Z123, by the Natural Science Foundation of China under Grant 60205002 and Grant 60875017, and by the Natural Science Foundation of Beijing under Grant 4042020. The authors would like to thank Dr. Daniel R. Treter and Professor Shiji Song for their help in revising this paper.

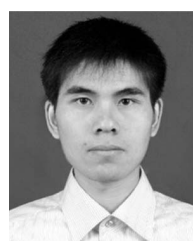
REFERENCES

- [1] D. Maltoni, D. Maio, A.K. Jain, and S. Probhaker, *Handbook of Fingerprint Recognition*. Springer-Verlag, 2003.
- [2] K. Karu and A.K. Jain, "Fingerprint Classification," *Pattern Recognition*, vol. 17, no. 3, pp. 389-404, 1996.
- [3] Q. Zhang and H. Yan, "Fingerprint Classification Based on Extraction and Analysis of Singularities and Pseudo Ridges," *Pattern Recognition*, vol. 37, no. 11, pp. 2233-2243, 2004.
- [4] B. Sherlock and D. Monro, "A Model for Interpreting Fingerprint Topology," *Pattern Recognition*, vol. 26, no. 7, pp. 1047-1055, 1993.
- [5] J. Gu and J. Zhou, "A Novel Model for Orientation Field of Fingerprints," *Proc. IEEE Int'l Conf. Computer Vision and Pattern Recognition*, vol. 2, pp. 493-498, June 2003.
- [6] A.K. Jain, S. Prabhakar, and L. Hong, "A Multichannel Approach to Fingerprint Classification," *IEEE Trans. Pattern Analysis and Machine Intelligence*, vol. 21, no. 4, pp. 348-359, Apr. 1999.
- [7] M. Tico and P. Kuosmanen, "A Multiresolution Method for Singular Points Detection in Fingerprint Images," *Proc. IEEE Int'l Symp. Circuits and Systems*, vol. 4, pp. 183-186, July 1999.
- [8] A.M. Bazen and S.H. Gerez, "Systematic Methods for the Computation of the Directional Fields and Singular Points of Fingerprints," *IEEE Trans. Pattern Analysis and Machine Intelligence*, vol. 24, no. 7, pp. 905-919, July 2002.
- [9] R. Cappelli, A. Lumini, D. Maio, and D. Maltoni, "Fingerprint Classification by Directional Image Partitioning," *IEEE Trans. Pattern Analysis and Machine Intelligence*, vol. 21, no. 5, pp. 402-421, May 1999.
- [10] P. Ramo, M. Tico, V. Onnia, and J. Saarinen, "Optimized Singular Point Detection Algorithm for Fingerprint Images," *Proc. IEEE Int'l Conf. Image Processing*, vol. 3, no. 3, pp. 242-245, Oct. 2001.
- [11] C.-H. Park, J.-J. Lee, M.J.T. Smith, and K.-H. Park, "Singular Point Detection by Shape Analysis of Directional Fields in Fingerprints," *Pattern Recognition*, vol. 39, no. 5, pp. 839-855, 2006.
- [12] X. Wang, J. Li, and Y. Niu, "Definition and Extraction of Stable Points from Fingerprint Images," *Pattern Recognition*, vol. 40, no. 6, pp. 1804-1815, 2007.
- [13] K. Nilsson and J. Bigun, "Complex Filters Applied to Fingerprint Images Detecting Prominent Symmetry Points Used for Alignment," *Proc. ECCV 2002 Workshop Biometric Authentication*, pp. 39-47, 2002.

- [14] K. Nilsson, "Symmetry Filters Applied to Fingerprints," PhD dissertation, Chalmers Univ. of Technology, 2005.
- [15] K. Nilsson and J. Bigün, "Localization of Corresponding Points in Fingerprints by Complex Filtering," *Pattern Recognition Letters*, vol. 24, no. 13, pp. 2135-2144, 2003.
- [16] S. Chikkerur and N.K. Ratha, "Impact of Singular Point Detection on Fingerprint Matching Performance," *Proc. Fourth IEEE Workshop Automatic Identification Advanced Technologies*, pp. 207-212, 2005.
- [17] P. Perona, "Orientation Diffusions," *IEEE Trans. Image Processing*, vol. 7, no. 3, pp. 457-467, 1998.
- [18] W. Fulton, *Algebraic Topology: A First Course*. Springer-Verlag, 1995.
- [19] M. Yawei and R. Luo, "Topological Method for Loop Detection of Surface Intersection Problems," *Computer-Aided Design*, vol. 27, no. 11, pp. 811-820, 1995.
- [20] G. Scheuermann, "Topological Vector Field Visualization with Clifford Algebra," PhD dissertation, Univ. of Kaiserslautern, Jan. 1999.
- [21] G. Scheuermann, H. Krüger, M. Menzel, and A.P. Rockwood, "Visualizing Nonlinear Vector Field Topology," *IEEE Trans. Visualization and Computer Graphics*, vol. 4, no. 2, pp. 109-116, Apr.-June 1998.
- [22] E.B. Saff and A.D. Snider, *Fundamentals of Complex Analysis with Applications to Engineering, Science, and Mathematics*, third ed. Prentice Hall, 2002.
- [23] A.M. Bazen, "Systematic Methods for the Computation of the Directional Fields and Singular Points of Fingerprints," *IEEE Trans. Pattern Analysis and Machine Intelligence*, vol. 24, no. 7, pp. 905-919, July 2002.
- [24] C. Burges, "A Tutorial on Support Vector Machines for Pattern Recognition," *Data Mining and Knowledge Discovery*, vol. 2, no. 2, pp. 121-167, 1998.
- [25] N. Cristianini and J. Shawe-Taylor, *An Introduction to Support Vector Machines*. Cambridge Univ. Press, 2000.
- [26] V. Vapnik, *The Nature of Statistical Learning Theory*. Springer, 2000.
- [27] A.K. Jain and L. Hong, "On-Line Fingerprint Verification," *IEEE Trans. Pattern Analysis and Machine Intelligence*, vol. 19, no. 4, pp. 302-314, Apr. 1997.
- [28] J. Zhou and J. Gu, "A Model-Based Method for the Computation of Fingerprints' Orientation Field," *IEEE Trans. Image Processing*, vol. 13, no. 6, pp. 821-835, June 2004.
- [29] J. Zhou and J. Gu, "Modeling Orientation Fields of Fingerprints with Rational Complex Functions," *Pattern Recognition*, vol. 37, no. 2, pp. 389-391, Feb. 2004.
- [30] C. Watson and C. Wilson, "NIST Special Database 4," *Fingerprint Database, Nat'l Inst. of Standards and Technology*, vol. 17, 1992.
- [31] D. Maio, D. Maltoni, R. Cappelli, J. Wayman, and A. Jain, "FVC2002: Second Fingerprint Verification Competition," *Proc. 16th Int'l Conf. Pattern Recognition*, vol. 3, pp. 811-814, 2002.



Jie Zhou received the BS and MS degrees from Nankai University, Tianjin, China, in 1990 and 1992, respectively, and the PhD degree from the Institute of Pattern Recognition and Artificial Intelligence, Huazhong University of Science and Technology (HUST), Wuhan, China, in 1995. From 1995 to 1997, he was a postdoctoral fellow in the Department of Automation, Tsinghua University, Beijing, where he is currently a full professor. His research area includes pattern recognition, image processing, computer vision, and information fusion. In recent years, he has authored more than 20 papers in international journals and more than 50 papers in international conferences. He received the Best Doctoral Thesis Award from HUST in 1995, the First Class Science and Technology Progress Award from the Ministry of Education (MOE) in 1998, the Excellent Teaching Award from Tsinghua University in 2003, and the Best Advisor Awards from Tsinghua University in 2004 and 2005, respectively. He was selected into the outstanding scholar plan of MOE in 2005. He is an associate editor for the *International Journal of Robotics and Automation* and *Acta Automatica Sinica*. He is a senior member of the IEEE.



Fanglin Chen received the BS degree from Xi'an Jiaotong University, Xi'an, China, in 2006. He is currently working toward the PhD degree in the Department of Automation, Tsinghua University, Beijing. His research interests are in pattern recognition, image processing, and computer vision.



Jinwei Gu received the BS and MS degrees from Tsinghua University, Beijing, in 2002 and 2005, respectively. He is currently working toward the PhD degree in the Department of Electrical Engineering, Columbia University, New York. His research interests are in pattern recognition, computer vision and graphics, and intelligent information processing. He has published more than 10 papers in international journals and international conferences. He is a student member of the IEEE.

▷ For more information on this or any other computing topic, please visit our Digital Library at www.computer.org/publications/dlib.